

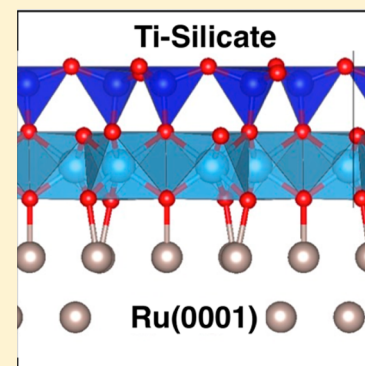
# Ultrathin Ti-Silicate Film on a Ru(0001) Surface

Frank Daniel Fischer,<sup>†</sup> Joachim Sauer,<sup>\*,†</sup> Xin Yu,<sup>§</sup> Jorge Anibal Boscoboinik,<sup>§</sup> Shamil Shaikhutdinov,<sup>\*,§</sup> and Hans-Joachim Freund<sup>§</sup>

<sup>†</sup>Institut für Chemie, Humboldt-Universität zu Berlin, Unter den Linden 6, 10099 Berlin, Germany

<sup>§</sup>Chemical Physics Department, Fritz-Haber-Institut der Max-Planck-Gesellschaft, Faradayweg 4-6, 14195 Berlin, Germany

**ABSTRACT:** Ultrathin Ti-silicate films were prepared on a Ru(0001) surface. Low-energy electron diffraction, scanning tunneling microscopy, and infrared reflection-absorption spectroscopy results support a structural model for the atomic structure of the films that is proposed using density functional theory calculations of films with varying Ti/Si ratios. The film segregates into a pure silicate and a Ti-silicate phase. According to the calculations, a uniform distribution of Ti in the silicate bilayer framework is energetically unfavorable. In the proposed structure, the Ti-silicate film with a Ti/Si 1:1 ratio consists of a monolayer of corner-sharing  $[\text{SiO}_4]$  tetrahedra on top of a monolayer formed by  $[\text{TiO}_6]$  octahedra. Ti–O–Ru bonds connect the film to the Ru substrate. Similar structures are known for both naturally occurring phyllosilicates and a recently reported Fe-silicate film.



## 1. INTRODUCTION

Well-defined ultrathin silicate<sup>1,2</sup> and aluminosilicate<sup>3,4</sup> films prepared on metal single-crystal support are of interest because they can be used to model, both experimentally and computationally, otherwise 3D complex materials such as zeolites.<sup>5,6</sup> Their advantage is that the virtually defect-free films can be investigated using the tools of surface science. The aluminosilicate film can be understood as the limiting case of a zeolite with infinite pore size and can therefore offer interesting opportunities to study structure–reactivity relationships of zeolites. Corner-sharing  $[\text{SiO}_4]$  tetrahedra form the formal building blocks of these films. By now, it is well known how under different experimental conditions either mono- or bilayers are formed.<sup>7</sup> Similar to the preparation of the Al-containing films, other metal cations can be incorporated into the films, as was most recently reported for the case of a Fe-containing silicate film.<sup>8</sup>

Here Ti-silicate films that were prepared following this same approach<sup>3</sup> are investigated. Titanium silicates or Ti-containing zeolites often find applications as catalysts. For example, titanium silicate-1 (TS-1), a structural analogue to the zeolite ZSM-5, where Ti is substituted for Al,<sup>9</sup> enabled new approaches for selective oxidation reactions.<sup>10</sup> Goodman and coworkers have previously deposited Ti onto a silica film grown on Mo(112) in their attempt to prepare  $\text{TiO}_2/\text{SiO}_2$  mixed oxide films.<sup>11</sup> They found that the  $\text{TiO}_x\text{-SiO}_2$  interfaces undergo significant restructuring upon annealing to temperatures above 1000 K such that  $\text{SiO}_2$  diffuses to the surface and becomes bonded via Si–O–Ti linkages. Note, however, that the authors discussed their results on the basis of a structural model of the monolayer silica film (so-called “cluster” model) that does not represent the true structure of the film (see more in ref 2).

We use density functional theory (DFT) to investigate possible substitution patterns of Ti in the silicate film as well as the structural and vibrational properties of the resulting films.

When replacing Si in silicates by metals, the question is always will the substitution be isomorph (as with Al)<sup>3</sup> or will a new structure type emerge (as with Fe).<sup>8</sup> Our DFT calculations show that the latter is the case and the Ti-containing films show a structural similarity to the Fe-containing silica films.<sup>8</sup> The Ti-silicate film consists of stacked silica and titanium oxide monolayer sheets (Ti/Si 1:1), where the Ti-containing layer is directly connected to the metal substrate via Ti–O–Ru bridges. This is an important contrast with the Al-distribution pattern in zeolites, which is governed by Loewenstein’s rule:<sup>12</sup> Al–O–Al connectivities are avoided, and Al atoms do not occupy neighboring tetrahedral sites.

## 2. METHODS AND MATERIALS

**2.1. Experiments.** The experiments were carried out in an ultrahigh vacuum (UHV) chamber equipped with low-energy electron diffraction (LEED, from Omicron), X-ray photoelectron spectroscopy (XPS) with a Scienta SES 200 hemispherical analyzer, infrared reflection-absorption spectroscopy (IRAS, Bruker IFS 66v), and scanning tunneling microscopy (STM, from Omicron). The Ru(0001) crystal (99.99%, from MaTeck) was mounted on an Omicron sample holder. The temperature was measured by a Type K thermocouple spot-welded to the edge of the crystal. The IRA spectra were recorded using p-polarized light at 84° grazing angle of

Received: May 5, 2015

Revised: June 11, 2015

Published: June 24, 2015

incidence (resolution  $4 \text{ cm}^{-1}$ ). STM images were obtained at room temperature using Pt–Ir tips.

The clean Ru(0001) surface was obtained by repeated cycles of  $\text{Ar}^+$ -sputtering and annealing to 1300 K in UHV. Then, the surface was precovered with a  $3\text{O}(2 \times 2)$ -layer by exposing to  $3 \times 10^{-6}$  mbar  $\text{O}_2$  at 1200 K for 5 min and cooling to 500 K prior to pumping oxygen out. For preparation of Ti-doped silica films, silicon and titanium were sequentially deposited onto the O/Ru(0001) surface at  $\sim 100$  K in  $2 \times 10^{-7}$  mbar  $\text{O}_2$  and annealed in  $5 \times 10^{-6}$  mbar  $\text{O}_2$  at  $\sim 1150$  K.

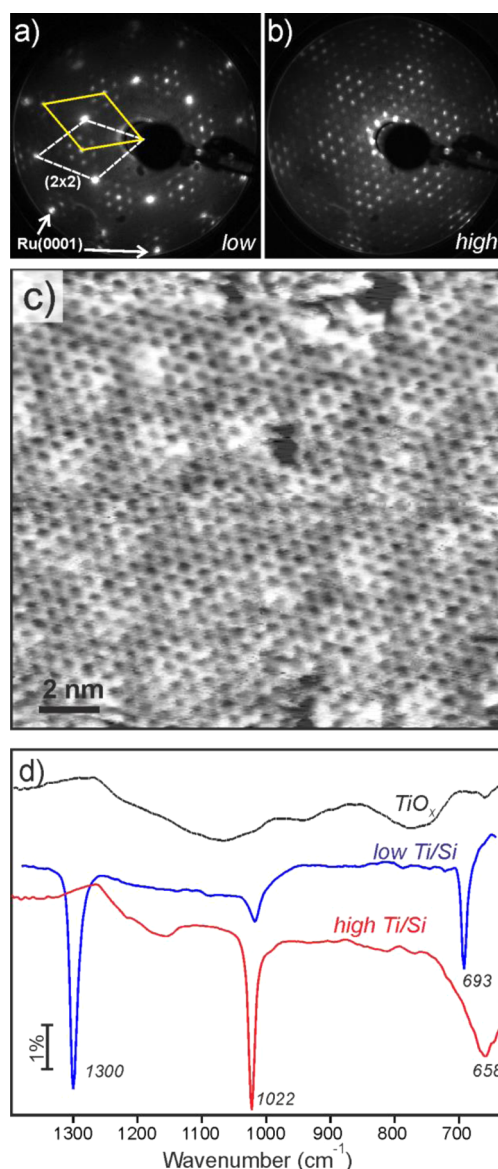
**2.2. DFT Calculations.** Periodic boundary conditions were applied and the Vienna ab initio simulation package (VASP)<sup>13,14</sup> was employed. The Perdew–Burke–Ernzerhof (PBE) functional<sup>15,16</sup> was used along with the projector-augmented wave (PAW) method.<sup>17,18</sup> A 400 eV cutoff for the plane-wave basis set and an  $8 \times 4 \times 1$  Monkhorst–Pack grid<sup>19</sup> for the integrations of the first Brillouin zone were used. The surface slabs were modeled using an orthogonal unit cell that is equivalent to the  $(2 \times 2)$  surface cell of Ru. The cell parameters of the silica double layer on Ru(0001),  $539.6 \times 934.6$  pm,<sup>20,21</sup> were used. The slabs consist of five Ru layers, with the three top layers allowed to relax and two bottom layers fixed to their bulk positions.

The positions of the nuclei were relaxed until the forces were  $< 0.005 \text{ eV/\AA}$ . For the calculation of the harmonic vibrational frequencies, we reoptimized the structures using the PBE functional augmented with a semiempirical  $1/r^6$  dispersion term (PBE+D).<sup>22,23</sup> A central finite difference method with 2.0 pm displacements in each Cartesian direction was used to obtain the frequencies. The intensities were obtained from the derivatives of the dipole moment component perpendicular to the surface. The vibrational frequencies are scaled by a factor of 1.0341, derived from a comparison between experimental and calculated frequencies for  $\alpha$ -quartz, to compensate for systematic errors of DFT and neglected anharmonicities.<sup>20</sup> The remaining deviations between calculated and experimental wavenumbers reflect the limits of this uniform scaling and the accuracy limits of DFT in general.

### 3. RESULTS AND DISCUSSION

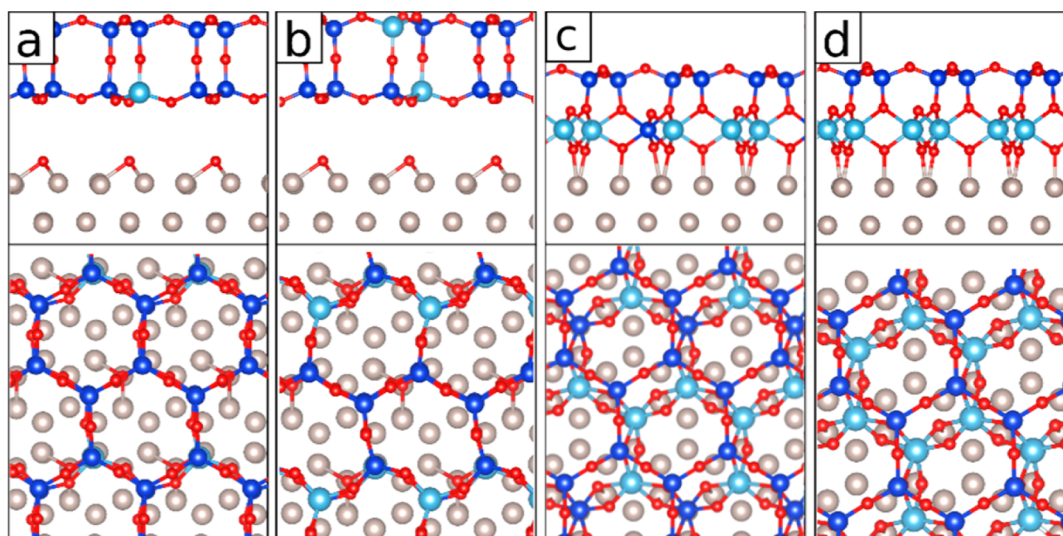
**3.1. Experimental Results.** Figure 1 summarizes LEED, STM, and IRAS results obtained on Ti-doped films prepared in the same way, as previously used for the preparation of the Fe-silicate films.<sup>8</sup> (See the Experimental Details.) The two films, presented in Figure 1, exhibit different Ti/Si ratios, noted here as “low” and “high” for comparison purposes only, as the precise ratios are difficult to determine by XPS due to strong overlapping of the Ti 2p and Ru  $3p_{3/2}$  signals. LEED patterns clearly indicate the formation of the well-ordered films. In addition to the pure silica surface that shows a  $(2 \times 2)$  symmetry with respect to the Ru(0001) surface, a new ordered structure develops as the Ti/Si ratio increases. The latter exhibits a shorter lattice constant ( $\sim 5.25 \text{ \AA}$ ) than the pure silica film ( $= 5.42 \text{ \AA}$ ) and is rotated by  $30^\circ$  with respect to the Ru(0001) surface. In addition, this new structure shows a Moiré-like coincidence superstructure, as evidenced by six satellite spots around each integer spot. A high-resolution STM image, shown in Figure 1c, reveals a honeycomb-like surface with a  $\sim 5.4 \text{ \AA}$  periodicity, which, in turn, exhibits a long-range (ca.  $22 \text{ \AA}$ ) modulation, in nice agreement with the LEED results.

Figure 1d presents the corresponding IRAS spectra, which are very sensitive to the principal structure of ultrathin silicate films,



**Figure 1.** (a,b) LEED patterns (60 eV) of the Ti-silicate films at low (a) and high (b) Ti content in the films. The unit cells are indicated. The principal spots of the Ru(0001) surface are marked by arrows. (c) High-resolution STM image of a Ti-silicate film showing a honeycomb-like surface structure. The Moiré structure resulting in a long-range surface modulation is also seen. Tunnelling conditions: sample bias 1.5 V, current 0.1 nA. (d) IRAS-spectra of the films corresponding to the LEED patterns in panels a and b. The spectrum for the  $\text{TiO}_x$  overlayer grown under the same conditions is also shown for comparison.

as previously shown.<sup>7</sup> The pure bilayer  $\text{SiO}_2$  film is characterized by very strong and sharp phonon bands at  $\sim 1300$  and  $\sim 693 \text{ cm}^{-1}$ , which are observed here also for the films at relatively low Ti/Si ratios (see a top spectrum); however, an additional band centered at  $1022 \text{ cm}^{-1}$  appears upon Ti doping, which dominates the spectrum at high Ti/Si ratio, whereas the spectral features of bilayer silica attenuate accordingly and disappear. Low-intensity spectral features in the frequency region below  $700 \text{ cm}^{-1}$ , which is near the absorption cut-edge of the KBr windows used in our spectrometer, were difficult to determine precisely in these experiments. For comparison, we have also examined a film



**Figure 2.** Top and side views of the most stable structures found by DFT at various Ti/Si ratios. (a)  $\text{TiSi}_7\text{O}_{16}\cdot 2\text{O}/\text{Ru}$ , (b)  $\text{Ti}_2\text{Si}_6\text{O}_{16}\cdot 2\text{O}/\text{Ru}$ , (c)  $\text{Ti}_3\text{Si}_5\text{O}_{16}\cdot 2\text{O}/\text{Ru}$ , and (d)  $\text{Ti}_4\text{Si}_4\text{O}_{16}\cdot 2\text{O}/\text{Ru}$ . Si, blue; Ti, light blue; O, red; Ru, gray.

formed only by Ti deposition under the same preparation conditions, which ultimately resulted in a  $\text{TiO}_x$  overlayer, which, as judged by STM, was very similar to the films reported by Männig et al.<sup>24</sup> These films did not show any IRAS features observed for the Ti-silicate films (not shown here). This finding rules out the formation of the alone-standing  $\text{TiO}_x$  structure in the resulting Ti-silicate films. Finally, water adsorption experiments on our Ti-silicate films revealed only silanol (Si–OH) groups.

**3.2. DFT Results.** **3.2.1. Structures.** The DFT modeling of the Ti-silicate film followed a methodology similar to the approach recently reported for the investigation of Fe-silicate films.<sup>8</sup> The bilayer silica film<sup>20,21</sup> with a  $\text{Si}_8\text{O}_{16}\cdot 2\text{O}/\text{Ru}(0001)$  composition was used as a starting point. Systematically, Ti atoms replaced one to four Si atoms of the bilayer unit cell. All possible structures of  $\text{TiSi}_7\text{O}_{16}\cdot 2\text{O}/\text{Ru}(0001)$ , formed by Ti substitution of one of the eight Si atoms in the unit cell, were examined. The structures were optimized. Subsequently,  $\text{Ti}_n\text{Si}_{8-n}\text{O}_{16}\cdot 2\text{O}/\text{Ru}(0001)$  structures were created by replacement of additional Si atoms in the most stable  $\text{Ti}_{n-1}\text{Si}_{8-(n-1)}\text{O}_{16}\cdot 2\text{O}/\text{Ru}(0001)$  structures, and their atomic positions were optimized. For  $\text{TiSi}_7\text{O}_{16}\cdot 2\text{O}/\text{Ru}$ , eight structures (substitution patterns) were examined. Seven structures were examined for  $\text{Ti}_2\text{Si}_6\text{O}_{16}\cdot 2\text{O}/\text{Ru}$ , 6 for  $\text{Ti}_3\text{Si}_5\text{O}_{16}\cdot 2\text{O}/\text{Ru}$ , and 16 for  $\text{Ti}_4\text{Si}_4\text{O}_{16}\cdot 2\text{O}/\text{Ru}$ , where some extra substitution patterns were taken into account in addition to those obtained by the procedure that was previously explained. The model system that was used for the calculations might introduce strain in the structure because the cell parameters are kept fixed. Because longer bond distances are expected for Ti–O bonds than for Si–O bonds, the cell volume should increase upon incorporation of Ti. For Ti-containing zeolites, de Man and Sauer found an increase in the cell volume with increasing Ti content.<sup>25</sup>

Figure 2 shows the most stable structures for each composition. The substitutions of one or two Si atoms by Ti per unit cell (u.c.) preserve the bilayer structure; that is, it is isomorphous. The energies per unit cell for all structures found were within 1.3 and 23 kJ/mol, respectively. The lowest energy structures found for  $\text{Ti}_3\text{Si}_5\text{O}_{16}\cdot 2\text{O}/\text{Ru}$  and  $\text{Ti}_4\text{Si}_4\text{O}_{16}\cdot 2\text{O}/\text{Ru}$  are qualitatively different. The energies per unit cell of the

structures shown in Figure 1c,d were 68 and 217 kJ/mol lower than structures with the same composition that did more closely resemble the original bilayer structure, similarly to those of lower Ti content.

Table 1 compares structural details of the pristine silica layer on top of the Ru(0001) surface with the global minimum

**Table 1. Comparison of Selected Distances (in pm) Calculated for  $\text{Si}_8\text{O}_{16}\cdot 2\text{O}/\text{Ru}$  and  $\text{Ti}_4\text{Si}_4\text{O}_{16}\cdot 2\text{O}/\text{Ru}^a$**

distance/pm	$\text{Si}_8\text{O}_{16}\cdot 2\text{O}/\text{Ru}$	$\text{Ti}_4\text{Si}_4\text{O}_{16}\cdot 2\text{O}/\text{Ru}$
$r(\text{O}_{\text{surface}}-\text{Ru})$	202–203	202–205
$r_z(\text{O}_{\text{surface}}-\text{Ru})^b$	117	200
$r_z(\text{O}_{\text{surface}}-\text{O}_{\text{layer}})^c$	322	
$r(\text{O}_{\text{surface}}-\text{Ti}_{\text{layer}})^d$		197–203

<sup>a</sup>Figure 2d. <sup>b</sup>Distance between the topmost layer of Ru atoms and the surface oxygen atoms. <sup>c</sup>Distance between the planes of the surface oxygen atoms and the bottom oxygen layer of the  $\text{SiO}_2$  film. <sup>d</sup>Ti–O bonds connecting Ti atoms to the bottom layer with surface oxygen atoms.

structure of  $\text{Ti}_4\text{Si}_4\text{O}_{16}\cdot 2\text{O}/\text{Ru}$  (Figure 2d), which does no longer resemble the bilayer structure. The topmost layer rather resembles silica monolayers, as observed on Ru(0001), Mo(112), and SiC(0001),<sup>2,7</sup> in which all Si atoms are four-fold coordinated to oxygen atoms. The bottom layer consists of edge-sharing  $[\text{TiO}_6]$  octahedra, which share corners with the  $[\text{SiO}_4]$  tetrahedra of the top layer. The three oxygen atoms of the  $[\text{TiO}_6]$  octahedra that are closest to the Ru surface are within 202–205 pm of the next Ru atoms, while their distance to Ti is 197 to 203 pm. (See Table 1.) In the case of the structure of  $\text{Ti}_4\text{Si}_4\text{O}_{16}\cdot 2\text{O}/\text{Ru}$ , the surface oxygen atoms and the oxygen atoms that originally belonged to the bilayer cannot be differentiated. The Ti atoms of the bottom layer are now connected to the Ru surface via oxygen atoms. This situation is shown in Figure 3.

Figure 3 demonstrates that there are three different types of O atoms connected to Ti atoms: (i) two-fold coordinated O atoms, connected to two Ti atoms; (ii) three-fold coordinated O atoms, connecting to two Ti atoms and one Si atom; and (iii) three-fold coordinated O atoms, connecting to two Ti

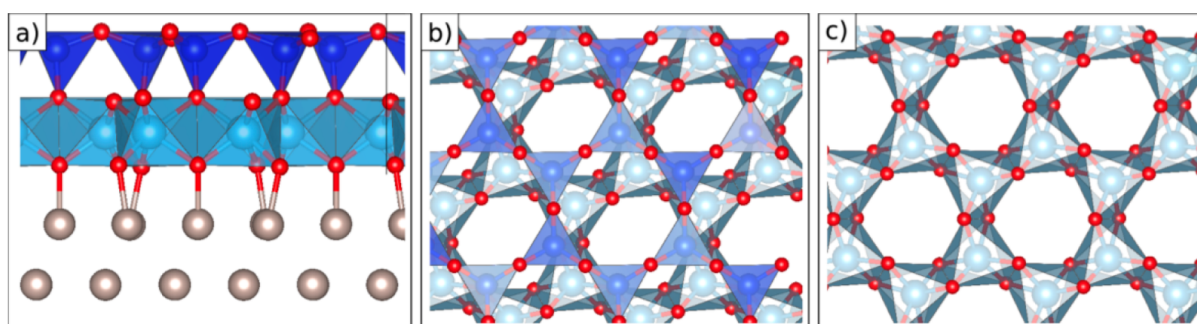


**Figure 3.** Views of the most stable structure found for the  $\text{Ti}_4\text{Si}_4\text{O}_{16}\cdot 2\text{O}/\text{Ru}$  unit cell. (a) Side view, polyhedral representation; Si, blue; Ti, light blue; O, red; Ru, gray. (b) Top view. (c) Top view of only the layer formed by  $[\text{TiO}_6]$  units.

atoms and one Ru atom of the metal surface. This is still in agreement with the assumption of formal charges for Ti and Si and for O. Formally, one might assign a charge of  $+2/3$  to each Ru atom that is directly connected to O. Obviously, the positive charge of the Ru substrate will be delocalized in the metal.

The theoretical prediction that Ti atoms occupy the bottom layer also agrees well with our water adsorption experiments, which showed only silanol groups  $\text{Si}-\text{OH}$  and no  $\text{Ti}-\text{OH}$ . (See Section 3.1.)

The proposed structure for the Ti-silicate film is reminiscent of layered silicates with  $\text{Si}_2\text{O}_5^{2-}$  formula unit, known as phyllosilicates. A typical case is talc,  $\text{Mg}_3\text{Si}_4\text{O}_{10}(\text{OH})_2$ , which is composed of  $\text{Si}_2\text{O}_5^{2-}$  sheets with  $\text{Mg}^{2+}$  ions sandwiched between sheets in octahedral sites (Figure 4).<sup>26</sup>

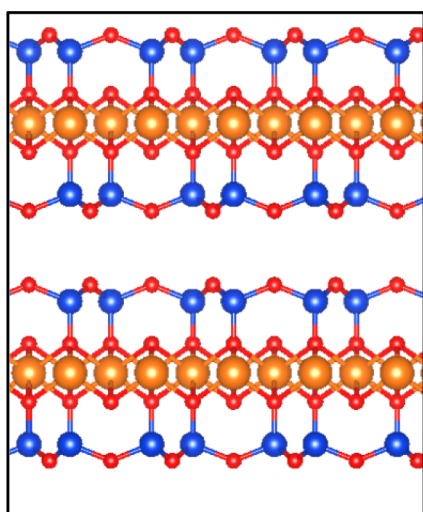


**Figure 4.** Crystal structure of talc,  $\text{H}_2\text{Mg}_3\text{O}_{12}\text{Si}_4$ , taken from ref 26. The positions of the hydrogen atoms are not shown. Si, blue; Mg, bronze; O, red.

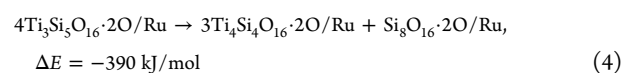
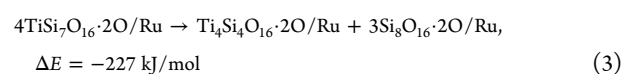
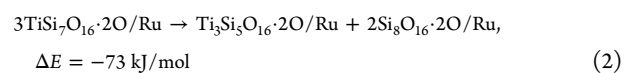
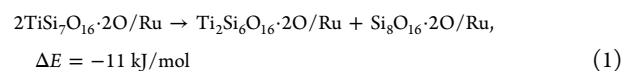
The silicate layer consists of interconnected six-membered rings of  $[\text{SiO}_4]$  tetrahedra extending outward to form the tetrahedral (T) layer. Every tetrahedron is connected to others by three of its oxygen atoms. The unshared oxygen atoms of all tetrahedra are orientated toward the same side, where the octahedral (O) layer is formed by the  $\text{Mg}^{2+}$  ions, with  $\text{OH}^-$  occupying two out of six corners of each octahedron. Each  $\text{OH}^-$  is shared by three of these octahedra. Apical oxygen atoms from the T layer above occupy two other corners; the remaining two are occupied by two apical oxygen atoms from the T layer below. Thus, an overall T–O–T sheet is formed

that interacts with other T–O–T sheets via weak van der Waals bonds.

Our  $\text{Ti}_4\text{Si}_4\text{O}_{16}\cdot 2\text{O}/\text{Ru}$  structure has obvious similarities to these systems. As can be seen in Figure 3, the Ti atoms are coordinated octahedrally, forming the O layer. Apical oxygen atoms of  $[\text{SiO}_4]$  tetrahedra of the layer above occupy two of the corners of the octahedra. This silica layer has the same structure as the T layer in phyllosilicates; it shares the overall composition of  $\text{Si}_2\text{O}_5^{2-}$ . Oxygen atoms that connect to the Ru substrate fill up the three remaining corners of the  $[\text{TiO}_6]$  octahedra. Instead of  $\text{OH}^-$  ions that are shared by three octahedra in the case of talc, there are now oxygen atoms, shared by only two octahedra.

Layered titanosilicates also appear in a class of minerals called heterophyllosilicates, such as bafertisite or nafertisite.<sup>27</sup> Like phyllosilicates, they have “T–O–T” sheets, but this and the general fact that titanium ions are included is the whole similarity to our  $\text{Ti}_4\text{Si}_4\text{O}_{16}\cdot 2\text{O}/\text{Ru}$  because in those heterophyllosilicates the  $\text{Ti}^{4+}$  ions do not form the centers of the octahedral layer. Rows of Ti-polyhedra are substituted periodically for rows of Si-tetrahedra within the tetrahedral layer.

**3.2.2. Stability.** For Fe-substituted silica films, phase separation into Fe-containing and pure silica domains has been observed.<sup>8</sup> To investigate possible analogous segregation behavior for the Ti-substituted films, we used total slab energies to estimate reaction energies for the following reactions



whereas reaction 1 shows a small energy gain for phase segregation into Ti-enriched ( $\text{Ti}_2\text{Si}_6$ ) and pure silica phases. Reactions 2 and 3 show a much larger energy gain for the segregation of layers with isolated tetrahedrally coordinated Ti atoms ( $\text{Ti}_7\text{Si}_7$ ) in the unit cell into a pure silica film and a film containing three and four, respectively, octahedrally coordinated Ti atoms in the bottom layer and four tetrahedrally coordinated Si atoms in the top layer. This energy gain is particularly large for the formation of the  $\text{Ti}_4\text{Si}_4$  film, which

results in a large energy gain also for the segregation of the  $\text{Ti}_3\text{Si}_5$  film into a  $\text{Ti}_4\text{Si}_4$  and a pure silica film. Therefore, even at low Ti content, the structural and spectral characteristics of the  $\text{Ti}_4\text{Si}_4$  film should be observed.

**3.2.3. Vibrational Spectra.** Figure 5 shows the harmonic IRA spectra simulated for the most stable  $\text{Ti}_4\text{Si}_4\text{O}_{16}\cdot 2\text{O}/\text{Ru}$

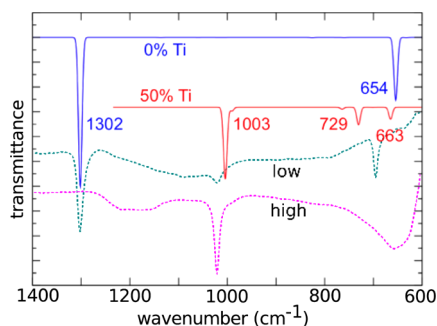


**Figure 5.** IRA spectra simulated for 0% Ti ( $\text{Si}_8\text{O}_{16}\cdot 2\text{O}/\text{Ru}$ ) and 50% Ti ( $\text{Ti}_4\text{Si}_4\text{O}_{16}\cdot 2\text{O}/\text{Ru}$ ). The spectra are scaled by a factor of 1.0341<sup>20</sup> and compared with experimental spectra at low and high Ti content.

structure (Figure 2d) and for the pristine silica bilayer. Only modes above  $600\text{ cm}^{-1}$  will be discussed here because only those can be compared with the experiment. The experimental spectra for low and high Ti content (see Figure 1d) are shown as dotted lines for comparison.

The peak at  $1302\text{ cm}^{-1}$  is very characteristic for the bilayer structure.<sup>7</sup> The corresponding vibrational mode is a symmetrical stretching of the interlayer Si–O–Si linkages. The band at  $654\text{ cm}^{-1}$  is a bending mode of the intralayer Si–O–Si bonds. The spectrum for the  $\text{Ti}_4\text{Si}_4\text{O}_{16}\cdot 2\text{O}/\text{Ru}$  system is qualitatively different. The most prominent vibrational mode at  $1003\text{ cm}^{-1}$  does not involve the Ti atoms that constitute the bottom layer. The mode solely describes a stretching of the Si–O bonds perpendicular to the surface that are part of the Si–O–Ti links between the upper silica layer and the bottom  $[\text{TiO}_6]$  layer (Figure 2d). This Si–O mode does not couple to the O–Ti mode because of the much higher mass of Ti compared with Si. Vibrational modes of similar frequencies were observed for silica monolayers grown on Mo(112) and Ru(0001).<sup>13</sup> The Fe-silicate film that has recently been reported exhibited a similar vibrational mode as well.<sup>8</sup>

#### 4. CONCLUSIONS

Combining experimental LEED, STM, and IRAS results with DFT structure and stability predictions resulted in an atomically resolved structure model of a well-ordered, ultrathin Ti-silicate film on a Ru(0001) surface. The film can best be described as a monolayer of corner-sharing  $[\text{SiO}_4]$  tetrahedra on top of a monolayer formed by  $[\text{TiO}_6]$  octahedra. The layers are connected by shared oxygen atoms at the corners of the  $[\text{SiO}_4]$  tetrahedra and  $[\text{TiO}_6]$  octahedra in the top and bottom layers, respectively. The  $[\text{TiO}_6]$  octahedra are connected to the Ru substrate via oxygen atoms shared by two Ti atoms and one Ru atom. The agreement of the calculated IRA spectra with the experimental ones provides compelling evidence of the proposed structural model and the segregation into pure silica and a 1:1 (Si/Ti) Ti-silicate phase. For low Ti contents, segregation is predicted and observed. Next to pristine silica bilayer domains, domains of the proposed Ti-silicate structure are formed. These results clearly differ from what was found for

Al substitution into pure silica films but are similar to what was recently found for Fe-containing silicate films.

#### AUTHOR INFORMATION

##### Corresponding Authors

\*Phone: +49 30 20937135. E-mail: js@chemie.hu-berlin.de.

\*Phone: +49 30 84134114. E-mail: shaikhutdinov@fhi-berlin.mpg.de.

##### Notes

The authors declare no competing financial interest.

#### ACKNOWLEDGMENTS

This work has been supported by a computer grant from the North German Computing Alliance Berlin–Hannover (HLRN) and by the German Research Foundation through Collaborative Research Center Grant CRC 1109). F.D.F. gratefully acknowledges a Kekulé scholarship by the Funds of the Chemical Industry. J.A.B. thanks the Alexander von Humboldt Foundation for the fellowship.

#### REFERENCES

- (1) Shaikhutdinov, S.; Freund, H. J. Metal-Supported Aluminosilicate Ultrathin Films as a Versatile Tool for Studying the Surface Chemistry of Zeolites. *ChemPhysChem* **2013**, *14*, 71–77.
- (2) Shaikhutdinov, S.; Freund, H. J. Ultrathin Silica Films on Metals: The Long and Winding Road to Understanding the Atomic Structure. *Adv. Mater.* **2013**, *25*, 49–67.
- (3) Boscoboinik, J. A.; Yu, X.; Yang, B.; Fischer, F. D.; Wlodarczyk, R.; Sierka, M.; Shaikhutdinov, S.; Sauer, J.; Freund, H. J. Modeling Zeolites with Metal-Supported Two-Dimensional Aluminosilicate Films. *Angew. Chem., Int. Ed.* **2012**, *51*, 6005–6008.
- (4) Boscoboinik, J. A.; Yu, X.; Emmez, E.; Yang, B.; Shaikhutdinov, S.; Fischer, F. D.; Sauer, J.; Freund, H. J. Interaction of Probe Molecules with Bridging Hydroxyls of Two-Dimensional Zeolites: A Surface Science Approach. *J. Phys. Chem. C* **2013**, *117*, 13547–13556.
- (5) Büchner, C.; Lichtenstein, L.; Yu, X.; Boscoboinik, J. A.; Yang, B.; Kaden, W. E.; Heyde, M.; Shaikhutdinov, S. K.; Wlodarczyk, R.; Sierka, M.; et al. Ultrathin Silica Films: The Atomic Structure of Two-Dimensional Crystals and Glasses. *Chem.—Eur. J.* **2014**, *20*, 9176–9183.
- (6) Sauer, J.; Freund, H. J. Models in Catalysis. *Catal. Lett.* **2015**, *145*, 109–125.
- (7) Yang, B.; Kaden, W. E.; Yu, X.; Boscoboinik, J. A.; Martynova, Y.; Lichtenstein, L.; Heyde, M.; Sterrer, M.; Wlodarczyk, R.; Sierka, M.; et al. Thin Silica Films on Ru(0001): Monolayer, Bilayer and Three-Dimensional Networks of  $[\text{SiO}_4]$  Tetrahedra. *Phys. Chem. Chem. Phys.* **2012**, *14*, 11344–11351.
- (8) Wlodarczyk, R.; Sauer, J.; Yu, X.; Boscoboinik, J. A.; Yang, B.; Shaikhutdinov, S.; Freund, H. J. Atomic Structure of an Ultrathin Fe-Silicate Film Grown on a Metal: A Monolayer of Clay? *J. Am. Chem. Soc.* **2013**, *135*, 19222–19228.
- (9) Taramasso, M.; Perego, G.; Notari, B. Preparation of Porous Crystalline Synthetic Material Comprised of Silicon and Titanium Oxides. U.S. Patent US 4410501 A, 1983.
- (10) Murugavel, R.; Roesky, H. W. Titanosilicates: Recent Developments in Synthesis and Use as Oxidation Catalysts. *Angew. Chem., Int. Ed.* **1997**, *36*, 477–479.
- (11) Chen, M. S.; Goodman, D. W. An Investigation of the  $\text{TiO}_x\text{-SiO}_2/\text{Mo}(112)$  Interface. *Surf. Sci.* **2005**, *574*, 259–268.
- (12) Loewenstein, W. The Distribution of Aluminum in the Tetrahedra of Silicates and Aluminates. *Am. Mineral.* **1954**, *39*, 92–96.
- (13) Kresse, G.; Furthmüller, J. Efficiency of Ab-Initio Total Energy Calculations for Metals and Semiconductors Using a Plane-Wave Basis Set. *Comput. Mater. Sci.* **1996**, *6*, 15–50.

- (14) Kresse, G.; Furthmüller, J. Efficient Iterative Schemes for Ab Initio Total-Energy Calculations Using a Plane-Wave Basis Set. *Phys. Rev. B* **1996**, *54*, 11169–11186.
- (15) Perdew, J. P.; Burke, K.; Ernzerhof, M. Generalized Gradient Approximation Made Simple. *Phys. Rev. Lett.* **1996**, *77*, 3865–3868.
- (16) Perdew, J. P.; Burke, K.; Ernzerhof, M. Generalized Gradient Approximation Made Simple (vol 77, pg 3865, 1996). *Phys. Rev. Lett.* **1997**, *78*, 1396–1396.
- (17) Blöchl, P. E. Projector Augmented-Wave Method. *Phys. Rev. B* **1994**, *50*, 17953–17979.
- (18) Kresse, G.; Joubert, D. From Ultrasoft Pseudopotentials to the Projector Augmented-Wave Method. *Phys. Rev. B* **1999**, *59*, 1758–1775.
- (19) Monkhorst, H. J.; Pack, J. D. Special Points for Brillouin-Zone Integrations. *Phys. Rev. B* **1976**, *13*, 5188–5192.
- (20) Löffler, D.; Uhlrich, J. J.; Baron, M.; Yang, B.; Yu, X.; Lichtenstein, L.; Heinke, L.; Buchner, C.; Heyde, M.; Shaikhutdinov, S., et al., Growth and Structure of Crystalline Silica Sheet on Ru(0001). *Phys. Rev. Lett.* **2010**, *105*.
- (21) Włodarczyk, R.; Sierka, M.; Sauer, J.; Löffler, D.; Uhlrich, J. J.; Yu, X.; Yang, B.; Groot, I. M. N.; Shaikhutdinov, S.; Freund, H. J., Tuning The Electronic Structure of Ultrathin Crystalline Silica Films on Ru(0001). *Phys. Rev. B* **2012**, *85*.
- (22) Grimme, S. Semiempirical GGA-Type Density Functional Constructed with a Long-Range Dispersion Correction. *J. Comput. Chem.* **2006**, *27*, 1787–1799.
- (23) Kerber, T.; Sierka, M.; Sauer, J. Application of Semiempirical Long-Range Dispersion Corrections to Periodic Systems in Density Functional Theory. *J. Comput. Chem.* **2008**, *29*, 2088–2097.
- (24) Männig, A.; Zhao, Z.; Rosenthal, D.; Christmann, K.; Hoster, H.; Rauscher, H.; Behm, R. J. Structure and Growth of Ultrathin Titanium Oxide films on Ru(0001). *Surf. Sci.* **2005**, *576*, 29–44.
- (25) deMan, A. J. M.; Sauer, J. Coordination, structure, and vibrational spectra of titanium in silicates and zeolites in comparison with related molecules. An ab initio study. *J. Phys. Chem.* **1996**, *100*, 5025–5034.
- (26) Grüner, J. W. The Crystal Structures of Talc and Pyrophyllite. *Z. Kristallogr.* **1934**, *88*, 412–419.
- (27) Ferraris, G.; Bloise, A.; Cadoni, M. Layered Titanosilicates - A Review and Some Results on the Hydrothermal Synthesis of Bafertsite. *Microporous Mesoporous Mater.* **2008**, *107*, 108–112.